

## Article

# Enhancing the Photoluminescence and Microstructural Transformations of $\text{Al}_2\text{O}_3$ /Glass–Ceramic Composite Coatings by Laser Irradiation

Julio Correa <sup>1</sup>, Jairo Murillo <sup>1</sup>, Javier Jurado <sup>1</sup>, Lina García <sup>1</sup>, Liliana Tirado <sup>2</sup>, Hernán Colorado <sup>3</sup>, Jesús Evelio Diosa <sup>4</sup>, Alessandro Chiasera <sup>5</sup> and Clara Goyes <sup>6,\*</sup>

<sup>1</sup> Semillero de Investigación en Materiales para Sistemas Energéticos Sostenibles, Universidad Autónoma de Occidente, 760030 Cali, Colombia; julio\_andres.correa@uao.edu.co (J.C.); jlmurillo@uao.edu.co (J.M.); jajurado@uao.edu.co (J.J.); lina\_maria.garcia@uao.edu.co (L.G.)

<sup>2</sup> Grupo de Optoelectrónica, Instituto Interdisciplinario de las Ciencias, Universidad del Quindío, 630002 Armenia, Colombia; litirado@uniquindio.edu.co

<sup>3</sup> Grupo de Metalurgia Física y Teoría de Transiciones de Fase GMTF, Universidad del Valle, 760032 Cali, Colombia; hernan.colorado@correounalvalle.edu.co

<sup>4</sup> Grupo de Transiciones de Fase y Materiales Funcionales, Centro de Excelencia en Nuevos Materiales (CENM), Universidad del Valle, 760032 Cali, Colombia; jesus.diosa@correounalvalle.edu.co

<sup>5</sup> IFN-CNR CSMFO Laboratory and FBK Photonics Unit, Povo, 38123 Trento, Italy; chiasera@fbk.eu

<sup>6</sup> Grupo de Ciencia e Ingeniería de Materiales, Universidad Autónoma de Occidente, 760030 Cali, Colombia

\* Correspondence: cegoyes@uao.edu.co; Tel.: +57-31808000 (ext. 11386)



**Citation:** Correa, J.; Murillo, J.; Jurado, J.; García, L.; Tirado, L.; Colorado, H.; Diosa, J.E.; Chiasera, A.; Goyes, C. Enhancing the Photoluminescence and Microstructural Transformations of  $\text{Al}_2\text{O}_3$ /Glass–Ceramic Composite Coatings by Laser Irradiation. *Appl. Sci.* **2021**, *11*, 5091. <https://doi.org/10.3390/app11115091>

Academic Editors: Anna Lukowiak, Wilfried Blanc and Maurizio Ferrari

Received: 28 February 2021

Accepted: 30 March 2021

Published: 31 May 2021

**Publisher's Note:** MDPI stays neutral with regard to jurisdictional claims in published maps and institutional affiliations.



**Copyright:** © 2021 by the authors. Licensee MDPI, Basel, Switzerland. This article is an open access article distributed under the terms and conditions of the Creative Commons Attribution (CC BY) license (<https://creativecommons.org/licenses/by/4.0/>).

**Abstract:** This work presents an analysis of the crystallization process and the influence of laser surface modification on the crystalline phases and optical responses of  $\text{Al}_2\text{O}_3$ /glass–ceramic coatings deposited on a brass substrate. We used a  $\text{CO}_2$  laser at different irradiation powers to change the structure of the superficial layer. The photoluminescence response enhanced the resolution of its line shape as the irradiation power increased. X-ray diffraction patterns exhibit the presence of different crystalline phases for the samples irradiated.

**Keywords:** sol–gel method; alumina; laser surface modification; silica-stabilized zirconia glass-ceramics

## 1. Introduction

Alumina ceramics have found, for a long time, several important technological applications in optical [1] and microelectronic components [2] as protective, decorative, wear-resistant, solid-state device applications [3,4] and anticorrosion coatings [5–7], due to their chemical inertness, good mechanical strength and high hardness, transparency and good insulating properties [8].

In particular, high-temperature applications represent a new challenge for alumina ceramic joints in many fields [9], especially for complex-shaped alumina ceramic components. It has been found that joining ceramics to themselves, or to metals, can be achieved by direct solid-state diffusion [10], joining with metallic interlayers [11] and joining using glass or glass–ceramic interlayers [9,12,13]. These processes depend on solid-state diffusion and the interface that is formed at high pressures and high temperatures. A high bonding temperature, high bonding load and excellent surface finish [9] are generally required for joining ceramics. Some problems reported are the low resistance to oxidation at high temperatures, in addition to relatively long processing times at high temperatures to ensure sufficient mutual diffusion.

Joining with glass and glass–ceramic fillers is more appropriate due to the excellent chemical compatibility and matched coefficient of thermal expansion (CTE) between glass filler and ceramics [9,12,14].  $\text{CaO}-\text{Al}_2\text{O}_3-\text{SiO}_2$  have been employed as fillers for joining alumina ceramics [15]. On the other hand,  $\text{CaO}-\text{Al}_2\text{O}_3-\text{SiO}_2-\text{TiO}_2$  glass ceramics are also

used [9]. Among the advantages of using glass ceramics is the ability to obtain higher crystallinity, which allows the joint to be used at higher temperatures.

Several studies address the silica-stabilized zirconia,  $\text{SiO}_2\text{-ZrO}_2$  glass-ceramic system, synthesized with the sol-gel method [16,17] and, like alumina, its applications are aimed at taking advantage of its thermal and optical properties, especially in thermal barrier coatings. To study new materials for joining alumina ceramics and new procedures, this work uses  $\text{SiO}_2\text{-ZrO}_2$  glass-ceramic fillers and a  $\text{CO}_2$  laser surface modification technique. The use of laser surface treatment techniques for the treatment of alumina coatings has been reported due to the high crystallinity that it confers on the material, and it has been shown that the required time is usually in the range of 1 to 15 min [15]. Further, laser treatment represents an optical technique to detect phase transformation and densification of  $\text{Al}_2\text{O}_3$  coatings. Laser surface modification of alumina coatings leads to the elimination of porosities and restoration of the stable phase [3,18].

This paper reports the spectroscopic properties of the  $\text{Al}_2\text{O}_3/\text{SiO}_2\text{-ZrO}_2$  glass-ceramic filler on the brass substrate, where the laser surface modification causes a phase transformation.

## 2. Materials and Methods

The  $\text{Al}_2\text{O}_3$ /glass-ceramic composite coating was deposited onto brass substrates by the sol-gel process. Before deposition of the glass ceramic, an alumina interlayer ( $\text{Al}_2\text{O}_3$ ) was deposited over the brass substrate using the standard air plasma spray technique to ensure the junction of the glass-ceramic layer. The brass substrates were cleaned by ultra-sound and alcohol without any special surface treatment. To achieve uniform porosity networks, we used a fused and crushed alumina powder (Metco 105&105SF).

For the preparation of the  $\text{ZrO}_2\text{-SiO}_2$  glass ceramic, silica was synthesized via acid hydrolysis of triethylorthosilicate (TEOS, Merck 98% purity), ethanol (Sigma-Aldrich, 99.5% purity), de-ionized water (Amresco) and nitric acid as the catalyst. The mixture was pre-hydrolyzed for 1 h at 70 °C, and it was maintained under these conditions for another 3 h to induce gelation. The molar ratio of TEOS:HNO<sub>3</sub>:EtOH:H<sub>2</sub>O was 0.1:0.00005:15.5:2.8. Pure zirconia was obtained from hydrolysis of two different precursors,  $\text{Zr}(\text{C}_3\text{H}_7\text{O})_4$  (Sigma-Aldrich) and  $\text{ZrClO}_2\cdot 8\text{H}_2\text{O}$  (Merck). The mixture was kept at 50 °C for 1 h under constant agitation. This suspension was then added to the TEOS solution, resulting in a Zr:Si molar ratio of 90:10, and maintained at 70 °C for 1 h. The preparation was deposited onto  $\text{Al}_2\text{O}_3$ /brass substrates (1 in diameter) by the spin-coating technique (Laurell technologies ws-650 series). We established the rotation speed at 500 rpm and the rotation time at 50 s.

The  $\text{Al}_2\text{O}_3/\text{ZrO}_2\text{-SiO}_2$  composite coating deposited on the brass substrate was then thermally treated at 850 °C for 60 min. Three samples were stabilized by a post-treatment using a  $\text{CO}_2$  laser. This laser (Boye Laser HSLC-1206) of 10.6 μm wavelength with a beam diameter of 6 mm was used for laser modification of the surface. The power density of the  $\text{CO}_2$  laser beam was 0.69 (SSZ01), 1.04 (SSZ02) and 1.38 W/cm<sup>2</sup> (SSZ03). The samples were positioned at around 50 cm from the laser output and exposed for 1 min. In Figure 1, we present the computer-aided design (CAD) for the laser annealing path (1 in<sup>2</sup>).

The photoluminescent signal was obtained by exciting the sample with the 488 nm line of an Argon laser. A 1 m focal distance spectrometer, with an 1800 g/mm grating and a thermoelectrically cooled CCD camera, was used to analyze the spectral response. The range for photoluminescence (PL) signal detection was between 550 and 900 nm.

The crystalline structure of the sample was investigated by X-ray diffraction (XRD). The diffractometer used was a Bruker D8 Advance with a vertical goniometer; the emission used was 1.5 angstrom radiation emitted by a Cu anode ( $K_\alpha$  line) using 35 mA for the filament current and 30 kV for electron acceleration. The detector was a NaI crystal coupled to a photomultiplier tube. A graphite monochromator was located before the detector to eliminate the Cu- $K_\beta$  line. The divergence and antiscattering slits used were 0.6 mm each and 0.1 mm for the detector slit. The microstructure of the samples was studied using a scanning electron microscope (SEM, Phenom PROX, Cali, Colombia).

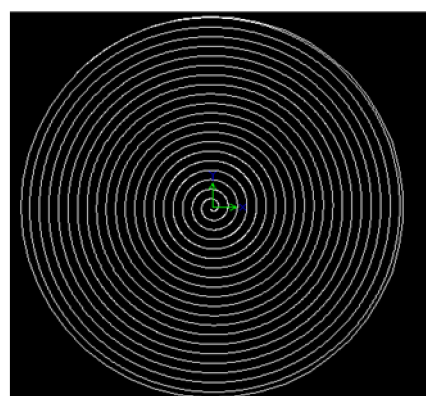


**Figure 1.** Computer-aided design image of the channel written with CO<sub>2</sub> laser system.

### 3. Results and Discussion

With the methodology described previously, we obtained regular coatings for all the thermally treated and laser-irradiated samples. The surface micrographs of the Al<sub>2</sub>O<sub>3</sub>/glass–ceramic coating are shown in Figure 2. The path laser is evident in the laser annealing surfaces. The laser path's definition on the surface is higher for higher laser density power (Figure 2c).

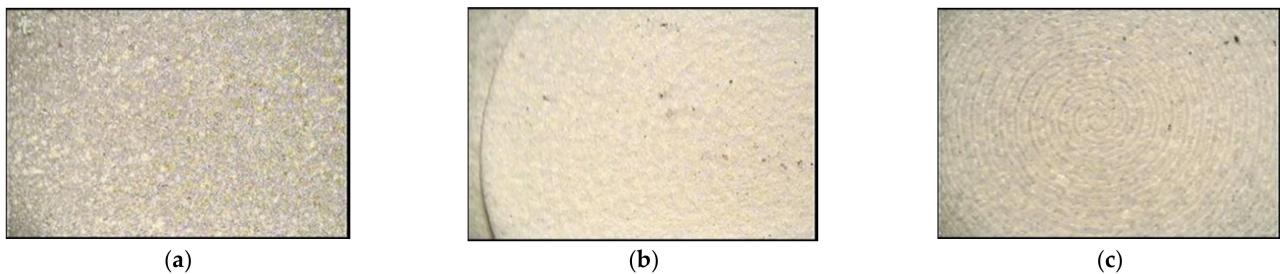


**Figure 2.** Imaging of the Al<sub>2</sub>O<sub>3</sub>/glass–ceramic composite coating, treated with different power densities of CO<sub>2</sub> laser irradiation: (a) without irradiation, (b) 0.69 W/cm<sup>2</sup> and (c) 1.04 W/cm<sup>2</sup>.

Figure 3 shows the surface morphology of the SSZ03 sample. The SEM images reveal a change in the surface profile created after laser irradiation on the Al<sub>2</sub>O<sub>3</sub>/glass–ceramic coating. The glass ceramic resembles a kind of broken glass on top of the alumina film. The coating layer's morphology is not uniform in the microscopic range, and the cracked surface is probably due to differences in the thermal behavior. The thickness of the alumina coating with similar manufacturing parameters is between 400 and 500 μm, as shown in Figure 4, in which the same authors have used Inconel 718 alloy as a substrate.

The SEM micrograph presented in Figure 5a corresponds to the surface image over the Al<sub>2</sub>O<sub>3</sub>/glass–ceramic coating. In two different positions on the surface, the composition is described by the EDS spectra (Figure 5b,c). It is evidenced that position 1 corresponds to the Al<sub>2</sub>O<sub>3</sub> layer and position 2 to ZrO<sub>2</sub>–SiO<sub>2</sub>.

Figure 6a corresponds to an image of a sample surface annealed by irradiation using 1.38 W/cm<sup>2</sup> of laser power density and following the design mentioned above. The surface exhibits differences between sections which are irradiated and those not irradiated. The modifications induced by the laser are structural, and the thermo-optic response supports this statement. Figure 6b shows the image obtained from the infrared emission induced by 520 nm radiation. In this map, the path pattern of the laser can be observed, showing the differences between the irradiated areas, as well as the homogeneity in the laser treatment carried out. This signal is associated with different non-radiative mechanisms and heat diffusion capabilities.

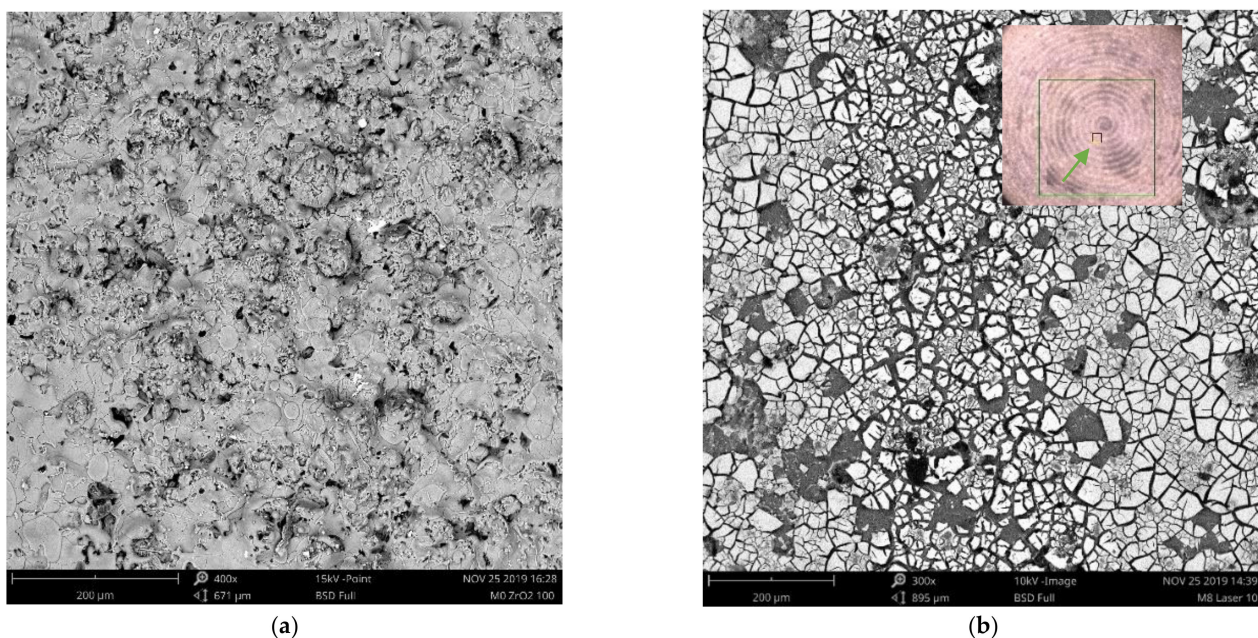


**Figure 3.** Scanning electron microscope (SEM) micrographs of the SSZ03 sample at different magnifications: (a) 400× and (b) 1620×.

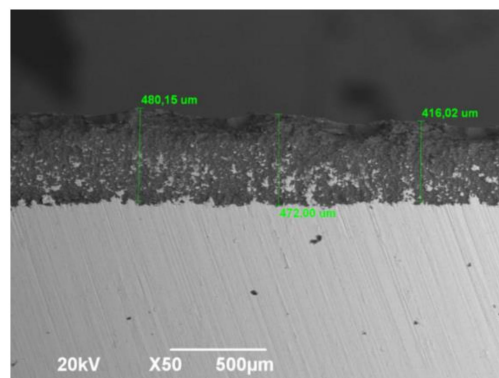


**Figure 4.** SEM micrographs of the alumina SEM image of alumina deposited on Inconel 718.

X-ray diffraction patterns of  $\text{Al}_2\text{O}_3/\text{SiO}_2\text{-ZrO}_2$  and  $\text{Al}_2\text{O}_3$  coatings both deposited on the brass substrate are presented in Figure 7. Figure 7a showed traces of tetragonal zirconia crystals at  $30.2^\circ$ ,  $50.4^\circ$ ,  $50.7^\circ$  ( $\theta$ ) reported in the JCPDS-ICDD data (set no. 50-1089). The tetragonal  $\text{ZrO}_2$  diffraction peaks correspond to the crystalline planes (011), (112) and (020), respectively, and the phase is conserved even when the sample reaches room temperature. Like the yttria-stabilized zirconia (YSZ), the most common material used as the ceramic layer, this demonstrates the well-known stabilizing effect in the  $\text{ZrO}_2$  structure, promoting the formation of high-purity tetragonal zirconia [19–21]. On the other hand, although the  $\text{Al}_2\text{O}_3$ /brass substrate sample displayed both  $\alpha$ -brass and  $\beta$ -brass phases, compared with the  $\text{Al}_2\text{O}_3/\text{SiO}_2\text{-ZrO}_2$ /brass substrate, only  $\alpha$ -brass was still observed [22]. This indicates that the  $\beta$ -brass is present or formed when the  $\text{Al}_2\text{O}_3$  is deposited ( $\gamma\text{-Al}_2\text{O}_3$ ), and when glass-ceramic and thermal treatment are used, this phase is transformed into  $\alpha$ -brass.

Figure 8 shows the X-ray diffraction patterns for the  $\text{Al}_2\text{O}_3$ /glass–ceramic composite coating system with different post-annealing treatments. Figure 8a shows only the sample annealed at  $850^\circ\text{C}$  at 60 min without any laser post-annealing; Figure 8b shows the sample annealed at  $850^\circ\text{C}$  at 60 min and under a  $\text{CO}_2$  laser using  $0.69\text{ W/cm}^2$  power density for 1 min; Figure 8c shows the sample annealed at  $850^\circ\text{C}$  and under a  $\text{CO}_2$  laser using  $1.04\text{ W/cm}^2$  power density for 1 min. All spectra display evidence of  $\text{ZrO}_2$  formation,

which is stable at ambient temperature. It is important to note that it was possible to obtain stable tetragonal  $\text{ZrO}_2$  in the  $\text{SiO}_2\text{-ZrO}_2$  coating by spin-coating and the thermal treatment applied at 850 °C for 60 min. The fitting procedure of the diffractograms indicates that the dominant structure is the tetragonal phase for  $\text{ZrO}_2$ , especially when  $\text{CO}_2$  laser irradiation energy is increased (to see  $2\theta = 30.2^\circ$ ).

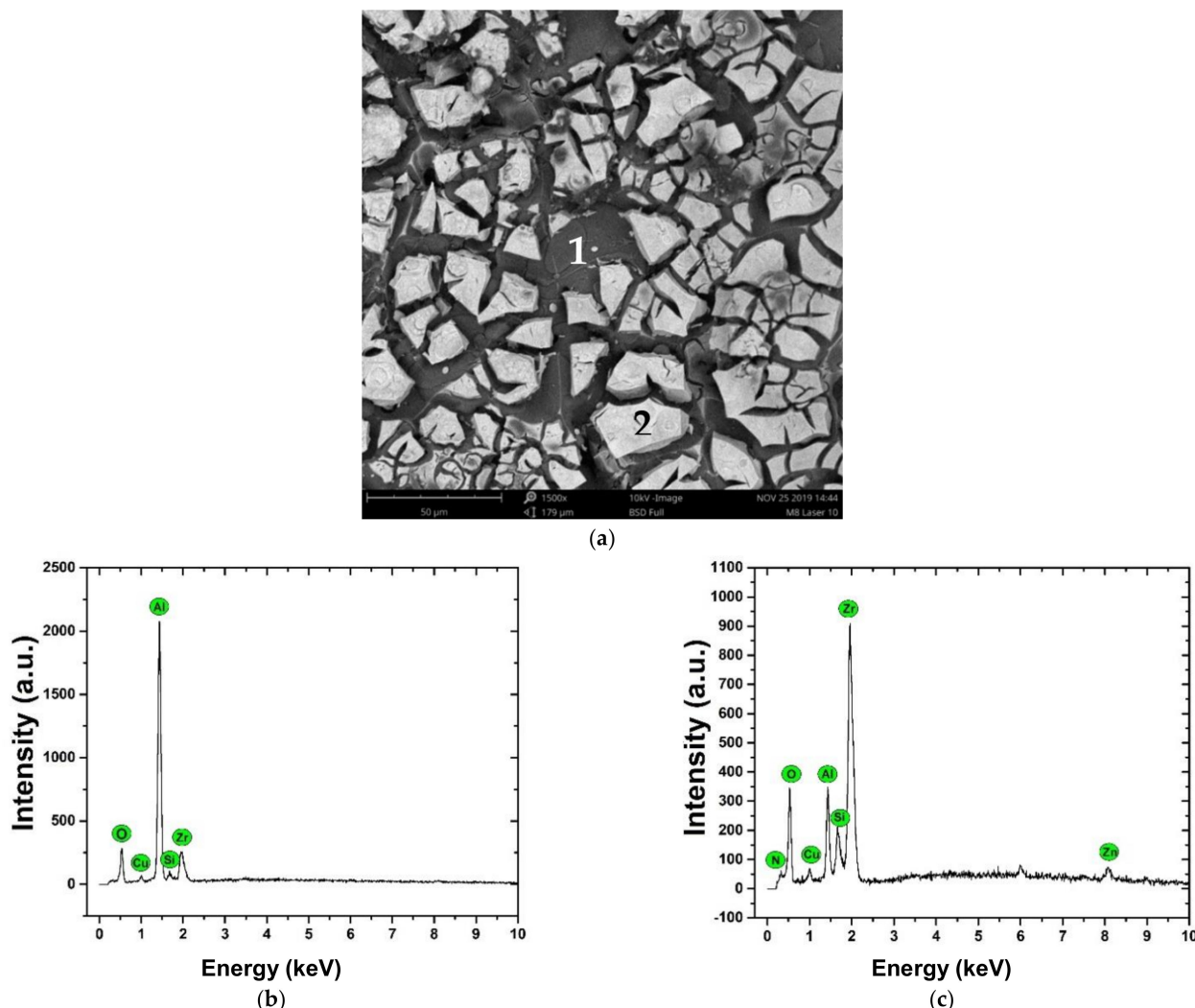


**Figure 5.** (a) SEM micrograph of the SSZ03 sample presenting position 1 and 2 for further EDS analysis, (b,c) EDS analysis over two different positions (1 and 2), respectively.

The sample annealed at 850 °C for 60 min (Figure 8a) in the oven shows differences from the same sample with  $\text{CO}_2$  laser post-annealing using  $0.69 \text{ W/cm}^2$  (Figure 8b) and  $1.04 \text{ W/cm}^2$  (Figure 8c) power density for 1 min. In Figure 8a, the as-sprayed  $\gamma\text{-Al}_2\text{O}_3$  is in a metastable phase, which is due to the rapid cooling rate of the process of plasma spraying, wherein alumina powder injected into the high temperature plasma is melted and entrained in the gas stream and is then accelerated and impinges on the substrate to form the coating [23].  $\text{CO}_2$  laser annealing allows the transformation of  $\gamma\text{-Al}_2\text{O}_3$  into thermodynamically stable  $\alpha\text{-Al}_2\text{O}_3$ , this transformation being more visible at higher power densities. Figure 8b,c show the XRD patterns typical of the stable corundum structure reported in JCPDS-ICDD data (set no. 46-1212).

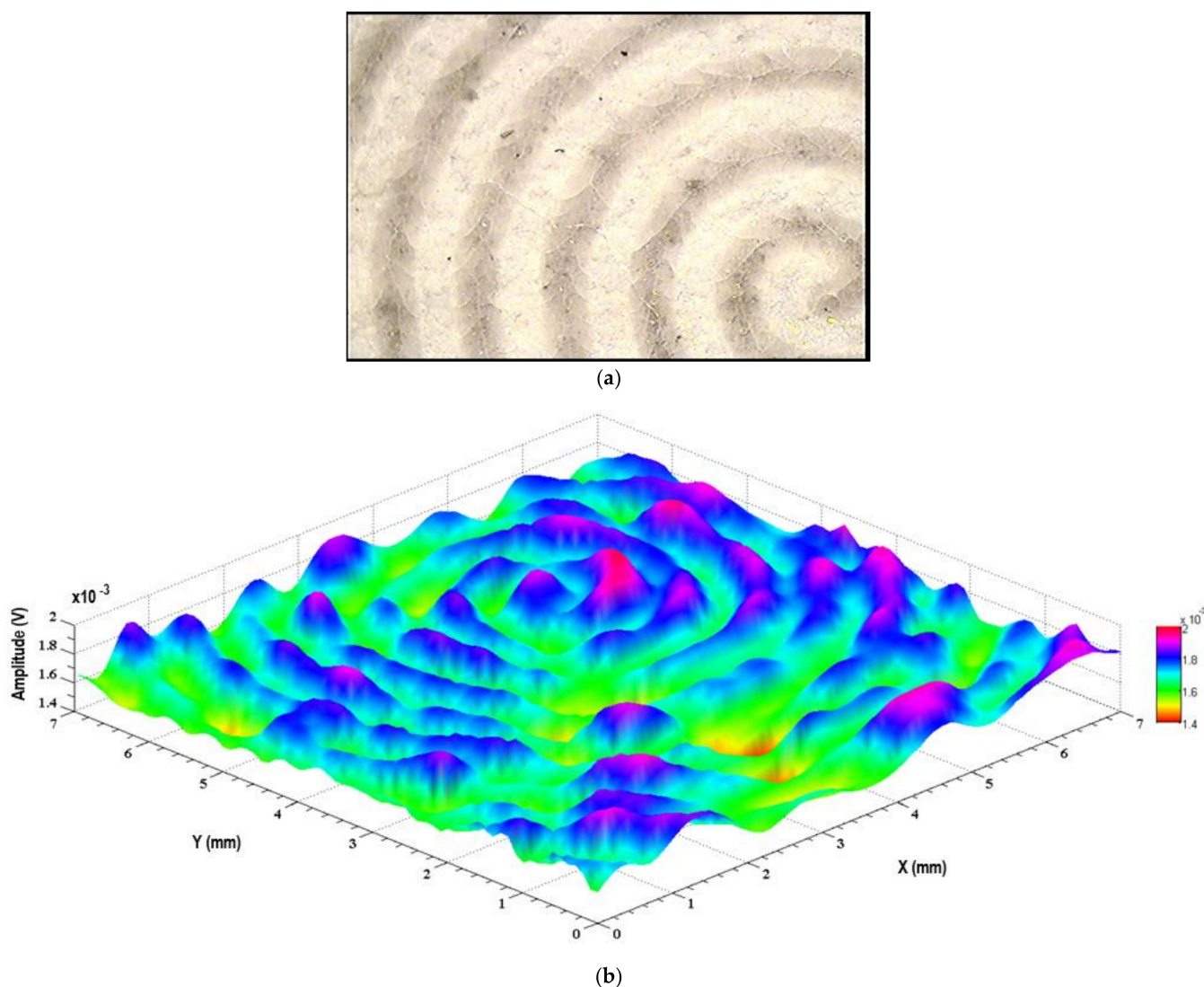


**Figure 6.** Surface morphology of the SSZ03 sample with laser annealing using  $1.38 \text{ W/cm}^2$  of power density: (a) optical microscopy image and (b) mapping of infrared emission induced by 520 nm radiation.

Figure 9 shows the PL spectra of  $\text{SiO}_2\text{-ZrO}_2/\text{Al}_2\text{O}_3$  coatings without laser post-annealing and annealed for 1 min with different laser power densities:  $0.69, 1.04, 1.38 \text{ W/cm}^2$ . In this figure, the effect of laser power on the optical response is shown. All annealed samples exhibit a doublet at around 694 nm and broad and weak emission bands at lower energies, in which intensities and sharpness are enhanced as the laser power increases. The origin of these emission bands is not yet established. We found reports that the spectral emission at higher energies is due to the F+ center (330 and 415 nm). Chromium impurity in the  $\text{Al}_2\text{O}_3$  lattice is characterized by two bands of absorption (3.1 and 2.2 eV), and one sharp emission structure peaked at 1.8 eV (696 nm), quite near the emission peak obtained by PL in this work [4,22]. According to this report, for the materials involved in the  $\text{Al}_2\text{O}_3$ /glass–ceramic composite coatings, the PL emission is associated with silica and zirconia in the  $\text{Al}_2\text{O}_3$  bond coat.

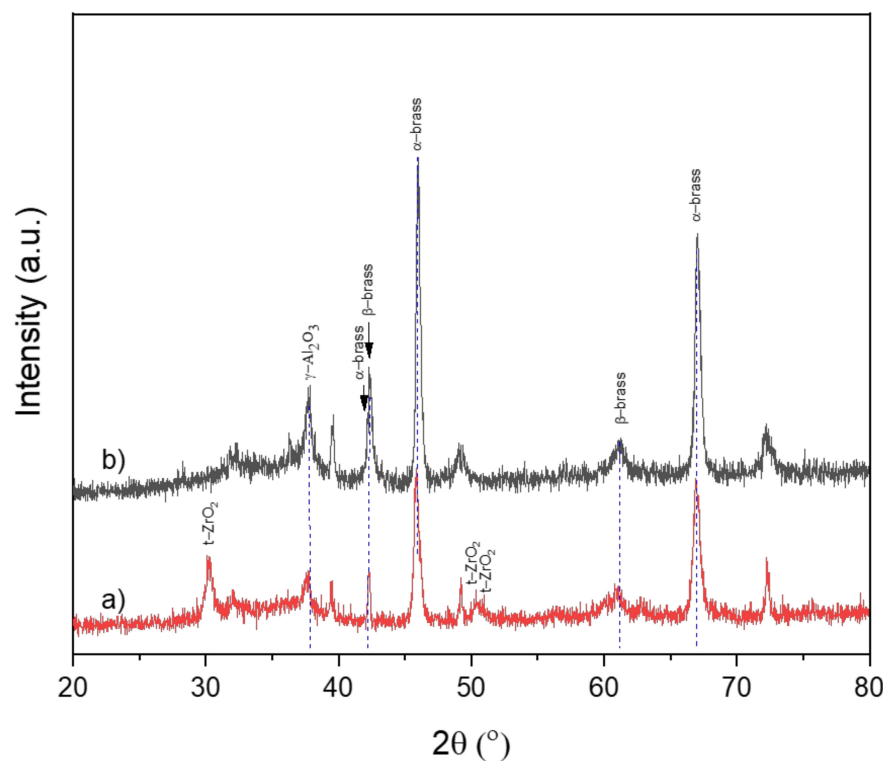


**Figure 7.** XRD pattern of (a)  $\text{Al}_2\text{O}_3/\text{SiO}_2\text{-ZrO}_2$  composite coating deposited on brass substrate annealed at  $850\text{ }^\circ\text{C}$ ; (b)  $\text{Al}_2\text{O}_3$  interlayer on brass substrate.

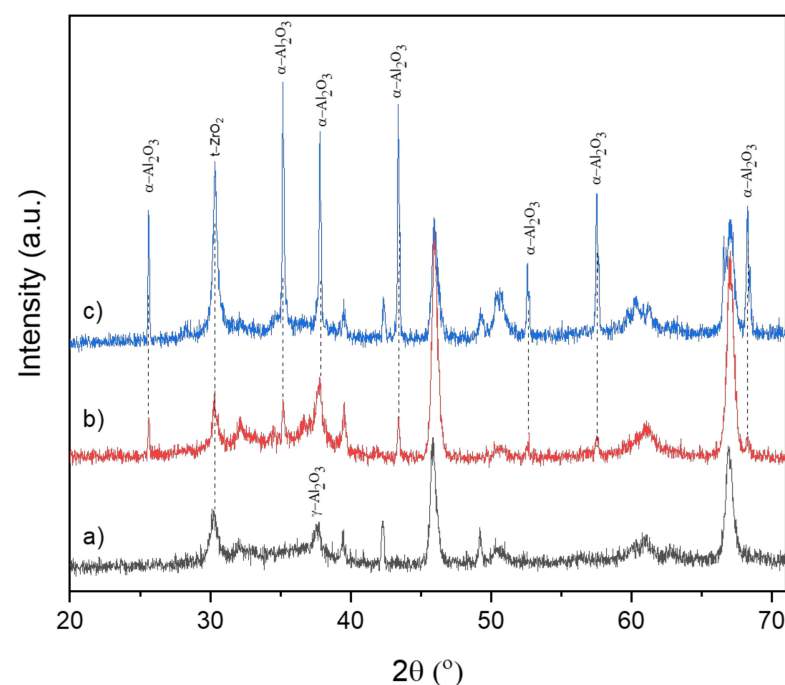


**Figure 8.** XRD pattern of  $\text{Al}_2\text{O}_3$ /glass–ceramic coating on  $\text{CuZn}$  substrate. (a) Only annealed at  $850\text{ }^\circ\text{C}$  at 60 min without any laser post-annealing; (b) annealed at  $850\text{ }^\circ\text{C}$  at 60 min and under  $\text{CO}_2$  laser using  $0.69\text{ W/cm}^2$  power density for 1 min; (c) annealed at  $850\text{ }^\circ\text{C}$  and under  $\text{CO}_2$  laser using  $1.04\text{ W/cm}^2$  power density for 1 min.

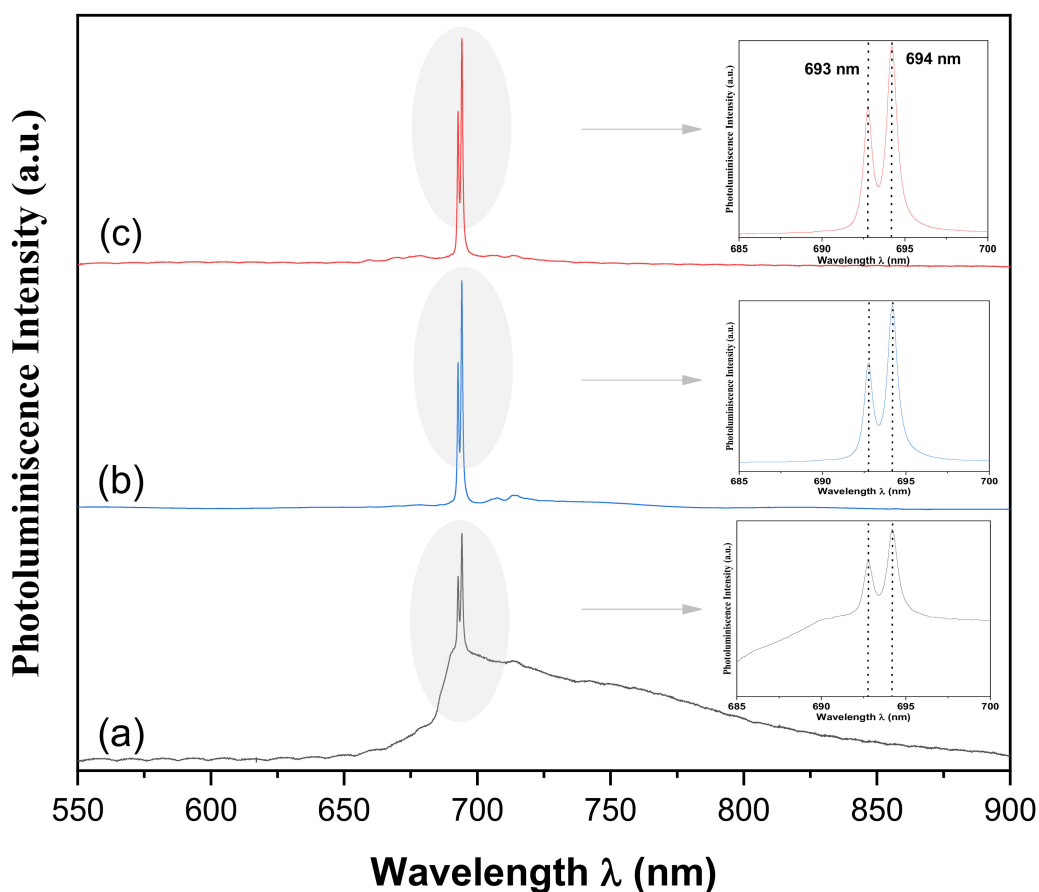


**Figure 9.** Photoluminescence spectra of  $\text{SiO}_2\text{-ZrO}_2$  with  $\text{CO}_2$  laser post-annealing for 1 min, using a power density of (a)  $0.69 \text{ W/cm}^2$ ; (b)  $1.04 \text{ W/cm}^2$  and (c)  $1.38 \text{ W/cm}^2$ .

#### 4. Conclusions

In this paper, we report the crystallization and the influence of laser surface modification on the crystalline phases and optical response of  $\text{Al}_2\text{O}_3$ /glass–ceramic coatings. The  $\text{ZrO}_2\text{-SiO}_2$  glass ceramic on alumina coatings prepared using the sol–gel technique, deposited under the experimental conditions used in this study, can be used for applications where a more stable alpha-alumina structure is required. This is due to the zirconia incorporated in the system maintaining its tetragonal phase at room temperature. This stable tetragonal  $\text{ZrO}_2$  phase at room temperature was obtained using annealing in an oven at  $850^\circ\text{C}$  in the  $\text{Al}_2\text{O}_3/\text{SiO}_2\text{-ZrO}_2$  composite coating.

Additionally, the results show that the use of  $\text{CO}_2$  laser annealing allows the identification of the spectroscopic properties of the studied system. In this sense, different power densities of  $0.69 \text{ W/cm}^2$ ,  $1.04 \text{ W/cm}^2$  and  $1.38 \text{ W/cm}^2$  were used to identify these properties. The annealing for 1 min allows the photoluminescence of the glass–ceramic system with optical emission to exhibit an intense double peak at  $693 \text{ nm}$  ( $1.789 \text{ eV}$ ) and  $694 \text{ nm}$  ( $1.786 \text{ eV}$ ) and weaker emission at lower energies. According to the surface micrographs and EDS analysis, the optical response is probably due to  $\text{Al}_2\text{O}_3$ , with a weak contribution of the  $\text{ZrO}_2\text{-SiO}_2$  glass ceramic at lower energies. Although the study had a very important focus on the phase transformation of alumina associated with heat treatment in furnaces and lasers, it can be shown that the entire studied system has a good response to  $\text{CO}_2$  laser annealing, since emission is well defined; thus, it could be of interest for various optical applications.

**Author Contributions:** Conceptualization, C.G.; methodology, J.C., J.M., J.J. and L.G.; investigation J.C.; formal analysis, L.T., H.C., J.E.D.; validation, A.C.; supervision, C.G.; resources, C.G., L.T., H.C., J.E.D. and A.C.; data curation, C.G.; writing—original draft preparation, C.G., L.T. and A.C.; writing—review and editing, C.G.; visualization, L.T. and A.C.; supervision, C.G.; project administration, C.G.; funding acquisition, C.G. All authors have read and agreed to the published version of the manuscript.

**Funding:** This research received no external funding.

**Institutional Review Board Statement:** Not applicable.

**Informed Consent Statement:** Not applicable.

**Data Availability Statement:** Not applicable.

**Acknowledgments:** The authors are grateful to the IIC radiometry laboratory of Universidad del Quindío and the Universidad Autónoma de Occidente for funding (Project code No. 17INTER-289).

**Conflicts of Interest:** The authors declare no conflict of interest.

## References

1. Aabid, A.; Khan, S.A. Optimization of Heat Transfer on Thermal Barrier Coated Gas Turbine Blade. *IOP Conf. Ser. Mater. Sci. Eng.* **2018**, *370*, 012022. [[CrossRef](#)]
2. Sankar, V.; Ramkumar, P.B.; Sebastian, D.; Joseph, D.; Jose, J.; Kurian, A. Optimized Thermal Barrier Coating for Gas Turbine Blades. *Mater. Today Proc.* **2019**, *11*, 912–919. [[CrossRef](#)]
3. Ghosh, S. Thermal properties of glass-ceramic bonded thermal barrier coating system. *Trans. Nonferrous Met. Soc. China* **2015**, *25*, 457–464. [[CrossRef](#)]
4. Adachi, S. Luminescence spectroscopy of Cr<sup>3+</sup> in Al<sub>2</sub>O<sub>3</sub> polymorphs. *Opt. Mater.* **2021**, *114*, 111000. [[CrossRef](#)]
5. Liu, B.; Liu, Y.; Zhu, C.; Xiang, H.; Chen, H.; Sun, L.; Gao, Y.; Zhou, Y. Advances on strategies for searching for next generation thermal barrier coating materials. *J. Mater. Sci. Technol.* **2019**, *35*, 833–851. [[CrossRef](#)]
6. Masalski, J.; Gluszek, J.; Nitsch, K.; Gluszek, P. Improvement in corrosion resistance of the 316L stainless steel by means of Al<sub>2</sub>O<sub>3</sub> coatings deposited by the sol-gel method. *Thin Solid Films* **1999**, *349*, 186–190. [[CrossRef](#)]
7. Cao, X.Q.; Vessen, R.; Stoever, D. Ceramic materials for thermal barrier coatings. *J. Eur. Ceram. Soc.* **2004**, *24*, 1–10. [[CrossRef](#)]
8. Guidi, F.; Moretti, G.; Carta, G.; Natali, M.; Rossetto, G.; Pierino, Z.; Salmaso, G.; Rigato, V. Electrochemical anticorrosion performance evaluation of Al<sub>2</sub>O<sub>3</sub> coatings deposited by MOCVD on an industrial brass substrate. *Electrochim. Acta* **2005**, *50*, 4609–4614. [[CrossRef](#)]
9. Zhu, W.; Zhang, H.; Xue, D.; Jiang, H.; Ran, X. Joining alumina ceramic by using glass ceramic filler with high crystallinity for high temperature application. *Ceram. Int.* **2019**, *45*, 20999–21003. [[CrossRef](#)]
10. Nagano, T.; Kato, H. Diffusion bonding of Zirconia/Alumina composites. *J. Am. Chem. Soc.* **1990**, *73*, 3476–3480.
11. Valette, C.; Marie-Francoise, D.; Voytovych, R.; Eustathopoulos, N. Interfacial reactions in alumina/CuAgTi braze/CuNi system. Interfacial reactions in alumina/CuAgTi braze/CuNi system. *Scr. Mater.* **2005**, *52*, 1–6. [[CrossRef](#)]
12. Wang, G.; Shan, Y.; Xu, J.; Chen, Y.; Li, J. Joining of AlON ceramics by using β-SiAlON/Y-Si-Al-O-N glass-ceramic as interlayer. *J. Non Cryst. Solids* **2019**, *503*, 389–396. [[CrossRef](#)]
13. Menzler, N.H.; Bram, M.; Buchkremer, H.P.; Stöver, D. Development of a gastight sealing material for ceramic components. *J. Eur. Ceram. Soc.* **2003**, *23*, 445–454. [[CrossRef](#)]
14. Döhler, F.; Kasch, S.; Schmidt, T.; Rüssel, C. Sealing of alumina using a CO<sub>2</sub> laser and a rapidly crystallizing glass. *J. Mater. Process. Technol.* **2016**, *233*, 206–211. [[CrossRef](#)]
15. Esposito, L.; Bellosi, A. Ceramic oxide bonds using calcium aluminosilicate glasses. *J. Mater. Sci.* **2005**, *48*, 2493–2498. [[CrossRef](#)]
16. Miranda-Salvado, I.M.; Serna, C.J.; Fernandez-Navarro, J.M. ZrO<sub>2</sub>-SiO<sub>2</sub> materials prepared by sol-gel. *J. Non Cryst. Solids* **1988**, *330*, 100. [[CrossRef](#)]
17. Wang, S.W.; Huang, X.X.; Guo, J.K. Mechanical properties and microstructure of ZrO<sub>2</sub>-SiO<sub>2</sub> composite. *J. Mater. Sci.* **1997**, *32*, 197. [[CrossRef](#)]
18. Thirumalaikumarasamy, D.; Shanmugam, K.; Balasubramanian, V. Corrosion performance of atmospheric plasma sprayed alumina coatings on AZ31B magnesium alloy under immersion environment. *J. Asian Ceram. Soc.* **2014**, *2*, 403–415. [[CrossRef](#)]
19. Goyes, C.; Ferrari, M.; Armellini, C.; Chiasera, A.; Jestin, Y.; Righini, G.C.; Fonthal, F.; Solarte, E. CO<sub>2</sub> laser annealing on erbium-activated glass-ceramic waveguides for photonics. *Opt. Mater.* **2009**, *31*, 1310–1314. [[CrossRef](#)]
20. Torres-Rodríguez, J.; Kalmář, J.; Menelaou, M.; Čelko, L.; Dvořák, K.; Cihlář, J.; Cihlář, J., Jr.; Kaiser, J.; Győri, E.; Veres, P.; et al. Heat treatment induced phase transformations in zirconia and yttria stabilized zirconia monolithic aerogels. *J. Supercrit. Fluids* **2019**, *149*, 54–63. [[CrossRef](#)]
21. Carpio, P.; Salvador, M.D.; Borrell, A.; Sánchez, E. Thermal behaviour of multilayer and functionally-graded YSZ/Gd<sub>2</sub>Zr<sub>2</sub>O<sub>7</sub> coatings. *Ceram. Int.* **2017**, *43*, 4048–4054. [[CrossRef](#)]

22. Ghannia, M.; Jardin, C.; Bouslama, M. Luminescent centres F and F+ in  $\alpha$ -alumina detected by cathodoluminescence technique. *J. Electron Spectrosc. Relat. Phenom.* **2003**, *133*, 55. [[CrossRef](#)]
23. Krishnan, R.; Dash, S.; Babu Rao, C.; Subba Rao, R.V.; Tyagi, A.K.; Raj, B. Laser induced structural and microstructural transformations of plasma sprayed  $\text{Al}_2\text{O}_3$  coatings. *Scr. Mater.* **2001**, *45*, 693–700. [[CrossRef](#)]